Helical Superstructure and Charged Polarons Contributions to Optical Non linearity of 2-Methyl-4-nitroaniline Crystals Studied by Resonance Raman, Electron Paramagnetic Resonance,...

ARTICLE *in* THE JOURNAL OF PHYSICAL CHEMISTRY A · JUNE 2011

Impact Factor: 2.69 · DOI: 10.1021/jp204168s · Source: PubMed

6 AUTHORS, INCLUDING:

Maria Magdalena Szostak
Wyższa Szkoła Handlowa we Wrocławiu
35 PUBLICATIONS **263** CITATIONS
SEE PROFILE

Krystyna Dyrek
Jagiellonian University
82 PUBLICATIONS **938** CITATIONS
SEE PROFILE

THE JOURNAL OF PHYSICAL CHEMISTRY A

ARTICLE

pubs.acs.org/JPCA

Helical Superstructure and Charged Polarons Contributions to Optical Nonlinearity of 2-Methyl-4-nitroaniline Crystals Studied by Resonance Raman, Electron Paramagnetic Resonance, Circular Dichroism Spectroscopies, and Quantum Chemical Calculations

M. Magdalena Szostak,*[,†] Henryk Chojnacki,[†] Katarzyna Piela,[†] Urszula Okwieka-Lupa,[†] Ewa Bidzińska,[‡] and Krystyna Dyrek[‡]

[†]Institute of Physical and Theoretical Chemistry, Wrocław University of Technology, Wybrzeże Wyspiańskiego 27, PL-50-370 Wrocław, Poland

[‡]Faculty of Chemistry, Jagiellonian University, ul. Ingardena 3, PL-30-060 Kraków, Poland

Supporting Information

ABSTRACT: The Raman excitation profiles of solid 2-methyl-4-nitroaniline (MNA) reveal several band enhancements by intermolecular and intramolecular charge transfer states. Calculated excited- and ground-state molecular geometries and excited state distortions qualitatively determined from Raman spectra indicate multiple vibrations leading to MNA dissociation. Also, overtones and combination tones can generate charged polarons, as detected by electron paramagnetic resonance after the exposure to 980 and 1550 nm laser diodes. The MNA space group *Ia* (C_s^4) is nonchiral; however, the electronic circular dichroism (CD) spectra of solution, KBr pellet, and single crystal were recorded. The crystal chirality is elucidated by room-temperature dynamic disorder, possible helical superstructure along the [102] polar axis, and charged polarons presence. The CD spectra ab initio calculations for MNA neutral and negatively charged monomers, dimers, and trimers, lying along the helix, confirmed the chirality. The role of these findings toward efficient optical nonlinearity and electric conductivity failure is discussed.

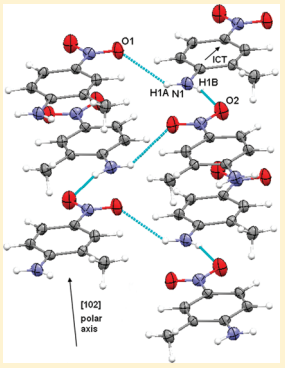

1. INTRODUCTION

The knowledge of electronic structure and excitations in organic molecules, molecular clusters and aggregates, in polymers and molecular crystals as well as in radical ions is essential for understanding their key properties for optoelectronics: optical nonlinearity and electric conductivity. The need for device miniaturization forces spatial arrangement studies because the structure shape decides the material functionality, like in the case of graphitic microtubules.[1] The often used methods of investigations are the electronic structure calculations like in the case of helical conducting polymers,[2] resonance Raman (RR) spectroscopy serving to characterize the vibronic couplings, for example, in helical porphyrin nanotubes,[3] and joint electronic absorption and circular dichroism (CD) spectra, for example, enabling to detect the three redox states, neutral, radical anion, and dianion, in chiral organogels serving as chirooptical switches in the visible and near-infrared (NIR) regions.[4] The time-dependent wave packet theory of spectroscopy[5] could describe in a consistent way electronic absorption and RR spectra and the first-order molecular hyperpolarisability (β), like in the case of large CT molecules.[6] Quantum dynamics theory including vibrational structure interpreted the electronic absorption and CD spectra of helical molecular aggregates.[7] The neutral 7,7,8,8-tetracyanoquinodimethane (TCNQ) molecule and its radical anion ($TCNQ^{-\cdot}$), the important electron acceptor components of organic CT conductors, were studied in solution by the RR spectra to find the π-bond order changes accompanying electron transfer.[8] Recently, the RR and optical absorption spectroscopies enabled authors to treat $TCNQ^{-\cdot}$ radical anion,[9] the nitroaromatic radical anions,[10] and *para*-phenylenediamine radical cation[11] as the ground-state mixed valence (intervalence) systems. Because of the classical theory of RR spectroscopy,[12] the presence of radical anions was detected in the TCNQ single crystal.[13] The RR spectra and quantum chemical calculations revealed the charge redistribution after deprotonation (in solution) of the push−pull 4-hydroxy-4′-nitroaminobenzene molecule reduced to its anion.[14] The common feature of conducting polymers,[15] radical ions,[4,8−10,14] and weakly conducting molecular crystals like TCNQ[16] and 3-nitroaniline (m-NA)[17] is the electronic absorption in NIR and/or IR regions important for telecommunication.[18] The NIR irradiation of m-NA crystals resulted in the generation and/or release from traps of paramagnetic species (radical anions, charged polarons);[17,19−21] in particular, the switching on/off of the 980 nm diode laser beam caused the sign reversal of crystal polarity.[21] The recently recorded and calculated CD spectra of m-NA solution and (nonchiral in theory) solids were explained by the helical

Received: May 5, 2011
Revised: May 31, 2011
Published: May 31, 2011

Scheme 1. 2-Methyl-4-nitroaniline (MNA) Molecule

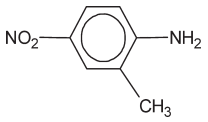

superstructure and charged polarons (radical anions) occurrence,[22] in accord with the theory of the CD spectra and the optical nonlinearity induced by the circularly polarized light absorbed by the spin-down and spin-up electrons in a different way.[23]

The radical anion presence in the crystal of push−pull, optically nonlinear 2-methyl-4-nitroaniline (MNA) molecule (Scheme 1), was deduced by us from the broad bands (at 0.53 and 0.82 eV) in polarized FT-NIR spectra and confirmed by their concentration determination (6×10^{15} spin/gram at room temperature) by the electron paramagnetic resonance (EPR).[24] By analogy to the optically nonlinear and weakly conducting m-NA crystal,[19,21] it was suggested that the MNA crystal is also a weak semiconductor in which protons could jump along one of the two distinct (3.097 and 3.246 Å) intermolecular N−H···O hydrogen bonds (HBs).[24] Like m-NA, MNA also became a model compound in nonlinear optics because of its efficient second harmonic generation (SHG)[25] and electrooptic Pockels effect.[26,27] The intramolecular charge transfer (ICT) and the noncentrosymmetric crystal packing were recognized early as the primary sources of MNA nonlinear optical (NLO) properties.[25,26,28−30] The estimation of the huge dipole moment enhancement (∼300%) by MNA crystal field,[31] reassessed as 30−40% 14 years later,[32] focused the theoreticians' interest on intermolecular interactions and their role toward the NLO properties.[33−37] The calculated singlet and triplet electronic transitions of isolated neutral MNA molecule and the doublet transitions of its radical ions were reported together with the low-temperature (5 K) emission spectra of MNA and 4-nitroaniline (p-NA) crystals.[38] The dynamic disorder above ∼90 K caused by the reorientational motions of all fragments of the MNA molecule in the solid state: $-NH_2$, $-NO_2$, $-CH_3$ groups, and phenyl rings, was found by variable temperature FT-IR and ^1H NMR methods.[39] The zigzag of molecules joined by the intermolecular HBs along the polar axis direction [102][30] suggested helical arrangement of molecules. On this basis, the hypothesis has been proposed that the dynamic disorder facilitates radical ions formation and induces the conformational chirality and CD of the MNA crystal.[39] MNA crystallizes with four molecules in a unit cell in the monoclinic nonconventional space group Ia[24,30] (equivalent to C_c and C^4 groups[25,26]) (point group m or C_s), and thus it does not belong to the chiral space groups.[40,41] Under certain conditions, it can reveal rotatory power.[42] The radical ion β values are often larger than these for the corresponding neutral molecules,[43,44] and thus they seem to be the intermediates in the molecular mechanism of optical nonlinearity.[43] This work was undertaken to check, both experimentally and theoretically, the hypotheses about the conformational and induced chirality of the MNA molecule and crystal, the generations and role of radical ions in the optical nonlinearity, and its electric conductivity.

2. EXPERIMENTAL AND COMPUTATIONAL METHODS

2.1. Measurements Setup. The commercial MNA (Aldrich) was purified, and the crystalline samples of MNA and of deuterated MNA (DMNA - with amine group deuterated in 85%) were obtained as described in ref 24. The Raman spectra of powdered (ground) MNA excited with eight lines (their powers in parentheses), 676.4 (15.7 mW), 647.1 (16.1 mW), 568.2 (11.6 mW), 530.9 (12.9 mW), 514.5 (13.8 mW), 496.5 (10.0 mW), 488.0 (12.3 mW) and 476.5 nm (4.0 mW), and 476.5 nm (4.0 mW), and of DMNA with three lines of an Ar−Kr ion laser (Spectra Physics) were recorded at 90° geometry at room temperature (RT) on a Jobin-Yvon T 64 000 spectrograph equipped with a liquid-N_2-cooled CCD camera at 2 cm^{-1} spectral resolution. The number of measured scans depended on the band intensity at given excitation line (e.g., two scans for 514.5 nm and 60 for 674 nm). The EPR spectra of MNA powders at RT were recorded on a Bruker Elexsys 500 spectrometer (Karlsruhe, Germany) operating in X-band (9.34 GHz) at a modulation frequency of 100 kHz, with modulation amplitude of 0.3 mT, microwave power of 3 mW, and four-fold accumulation. EPR parameters were read from spectrometer. The CD spectra of 0.026 M solution in the spectral grade chloroform and of MNA pellet pressed with KBr (5:250 mg/mg) and of MNA thin (∼0.01 cm) single crystal were measured on a JASCO J-75 spectropolarimeter with a xenon lamp. In the case of pellet, eight records were made by rotating the disk four times by 90° and by alternating the disk face,[45] whereas for the crystal plate, five spectra for different orientations were measured. Laser diodes (1550 nm, 50 mW) and (980 nm, 1 W) used to the NIR exposure (their choice will be addressed in Section 3.2) were positioned during irradiations 1 cm above the samples just before subjecting them to the EPR and CD spectrometers.

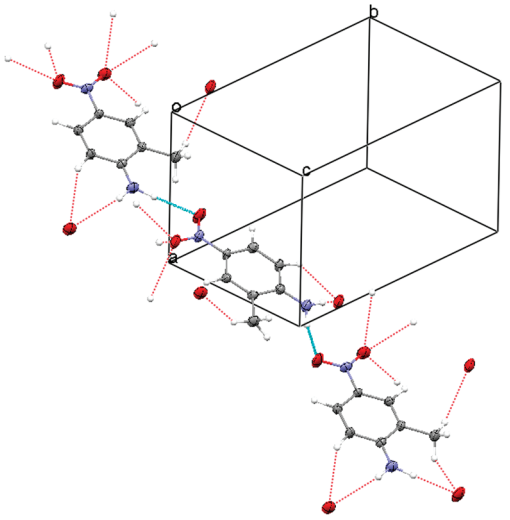

Figure 1. View of the MNA three molecules cluster along the polar axis [102],[30] presumably forming a helix (crystallographic data from ref 24).

2.2. Quantum Chemical Calculations. The UV−vis absorption and electronic CD spectra were first calculated for the MNA isolated molecule (fully optimized molecular geometry) and for a molecule with an electron attached (radical anion). Then, the electronic structure, static hyperpolarizabilites, ionization energies (IEs), electron affinities (EAs), and UV−vis and CD spectra of one neutral molecule (monomer), of neutral dimer and trimer, of MNA radical anion, and of MNA two and three molecules clusters with one electron added all lying along the [102][30] direction (Figure 1) were calculated by using Gaussian 09 package[46] within the cc-pVDZ basis set and hybrid B3LYP density functional, whereas CD spectra were calculated with

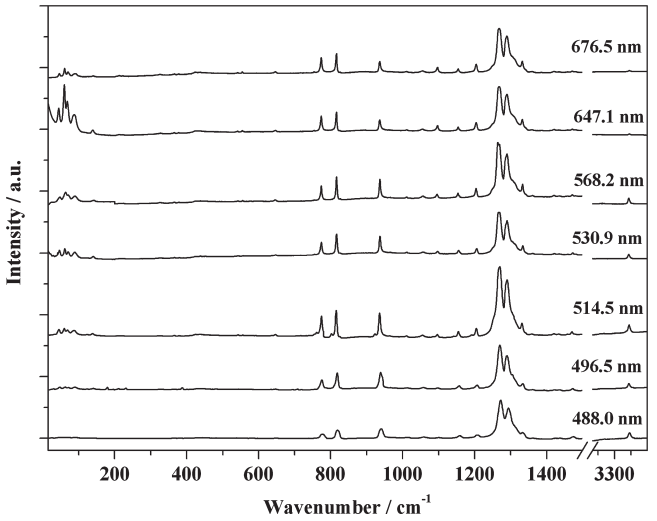

Figure 2. Raman spectra of powdered MNA in 10−3600 cm^{-1} range excited with different lines.

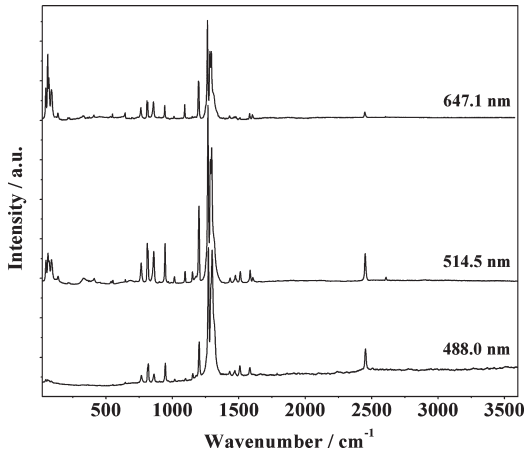

Figure 3. Raman spectra of powdered DMNA in 10−3600 cm^{-1} range.

the ORCA ab initio program with the same basis and density functional.[47] The optimized MNA molecular structures in the ground and the lowest excited singlet states have been evaluated with the SAC−CI (symmetry adapted cluster) method[48] based on the Gaussian program.[46] In this case, the 3-21 G basis set was used. The bandwidths of valence and conduction bands were calculated in different crystal directions within the semiempirical all-valence formalism, which is in fact the extended Hückel theory (EHT) method formulated for 1D crystal[49] and now reformulated for purposes of this work. It is because of the large molecular system under consideration (76 atoms in the unit cell, 252 orbitals even in the case of minimal basis set). The MNA atom coordinates were taken from the latest crystal structure.[24] The distance for transfer integrals taken into account in all cases was <20 Å.

3. RESULTS AND DISCUSSION

3.1. Resonance Raman and UV−vis Absorption Spectra. The MNA Raman spectra in the 10−3600 cm^{-1} range, taken with seven excited lines (the 476 nm causes damages of material) are shown in Figure 2. The DMNA spectra, recorded with three exciting lines, are presented in Figure 3. The parts of electronic

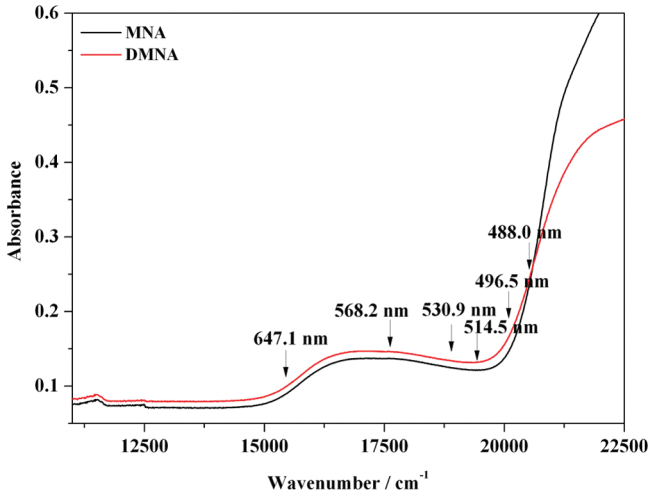

Figure 4. Electronic absorption spectra of MNA and DMNA thin films with marked wavelengths of laser lines used to excite the spectra.

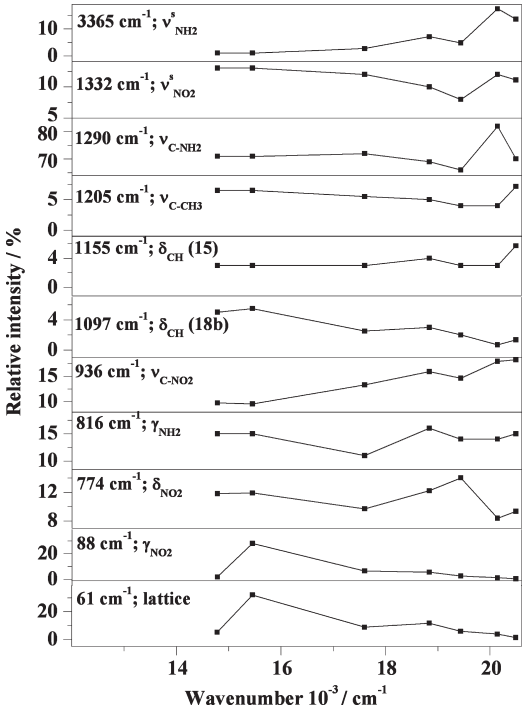

Figure 5. Excitation profiles for MNA chosen vibrational bands. The lines are only guides for eyes. Wavelengths of laser beams used, corresponding to experimental points, from left to right, are: 676.5, 647.1, 568.2, 530.9, 514.5, 496.5, and 488.0 nm.

absorption spectra of the MNA and DMNA thin layers, reported in ref 24, here with the arrows indicating wavelengths of excitation lines used, are shown in Figure 4. The weak bands at 16 530 (2.05 eV = 605 nm) and 15 750 cm^{-1} (1.95 eV = 635 nm)[24] were supposed to originate from the intermolecular CT calculated (CIS/INDO/S approximation) by Guillaume et al. for the MNA unit cell at 2.05 eV and at lower energies for the larger clusters along the *a* axis.[35] The ab initio calculated S_0-S_1 values for clusters composed of one, two, and three molecules along the polar [102] axis direction are equal to 3.63, 2.19, and 2.16 eV, respectively. The last two values are slightly larger than those of

Guillaume et al. The calculations for larger clusters exceeded computation possibilities. The relative intensities for 11 intense and isolated (with the exception of nonisolated $\nu^s_{NO_2}$ band at 1332 cm^{-1}) bands were estimated by taking as the internal standard (100%) at each exciting line the integral intensity of the 1267 cm^{-1} band (stretching ν_{CC}[24] (ν_{14})[50] vibration), similarly to the case of CT molecules[6] and conducting solid TCNQ salts.[51]

The excitation profiles for MNA vibration bands are presented in Figure 5; the corresponding bands for DMNA reveal the same features with the exceptional absence of $\nu^s_{NO_2}$ bands at all exciting lines. The positions and relative intensities of the vibrational bands shown in Figure 5 are given in Supporting Information, Table S1. The clearest enhancement of band intensities is seen in the case of low frequency (lattice and $-NO_2$ group out of plane vibrations) bands in the spectra excited with 647.1 nm line. We interpret the enhancement as arising from the coupling with intermolecular CT transition at 635 nm (Figure 4). The lack of low-frequency bands in the spectra excited with 496.5 and 488 nm lines may result from the different (intramolecular) electronic transitions in this region and from possible damages of the crystal structure. The strongest enhancement by the line 496.5 nm of the symmetric stretching vibration (3365, 1332, and 1290 cm^{-1} in Figure 5) bands of electron donor and acceptor groups confirms the ICT character of MNA n-π^* electronic transition lying at the edge of main absorption band in crystal at 21 400 cm^{-1} (2.65 eV = 468 nm)[38] not far from 459 nm.[52] The ab initio calculated S_0-S_1 transition energy for the molecule in optimized geometry is slightly lower than the value observed in the gas spectrum at RT (3.79 vs 4.2 eV)[53] and very similar to the value 3.82 eV.[38] Because the ICT in DMNA is weaker, the $\nu^s_{NO_2}$ bands are absent in its RR spectra. The enhancement of the MNA bands at 1205 and 1155 cm^{-1} by 488 nm line suggests that the next electronic transition originates from $\pi-\pi^*$ excitation in the phenyl ring. According to the time-dependent theory,[5,6,9,54] the modes of vibrations giving the most intense bands in Raman and RR spectra are responsible for the largest distortions (largest displacements of the excited-state potential surface along their normal coordinates).[6,54] The calculated (at 0 K) distances between chosen atoms in the MNA molecule ground and first excited states (in parentheses), differing mostly, are as follows: C−N(O_2) 1.447 Å (1.440 Å), C−N(H_2) 1.369 Å (1.379 Å), N−O 1.266 Å (1.347 Å), N−O′ 1.265 Å (1.425 Å), and C5−C6 1.380 Å (1.389 Å).

The MNA fluorescence and phosphorescence low-temperature (5 K) spectra reveal similar 1200 cm^{-1} vibronic progression, suggesting the coupling to symmetric stretching vibration of $-NO_2$ group and the zwitterionic structure in both ground and first excited singlet and triplet states.[38] The distances in the excited state confirm the vibronic couplings in the emission spectra and those observed in the RR spectra (at RT), especially for the $-NO_2$ group vibrations. It seems that the multiple fundamental MNA vibrations as well as the lattice modes can distort the geometry of excited electronic states and lead to the dissociation into radical ions. The decay of vibronic structures above 30 K[38] and all substituent group reorientations above 90 K[39] suggest that at RT the multidimensional distortions of excited states are more probable than those at low temperature. The crystal-point group symmetry at RT is very close to *mm*2 (C_{2v})[28] and presumably due to the atomic motions,[39] also, the average molecular symmetry increases. This assumption is in line with the small number of bands observed in the RR spectra as if they originate only from the totally symmetric modes (A_1 in C_{2v} point group symmetry). The mostly enhanced vibrations may lead to dissociation into radical ions. In the crystal, the collective excitations propagate as the excitons, here as the CT excitons, which because of the couplings with phonons became charge separated states.

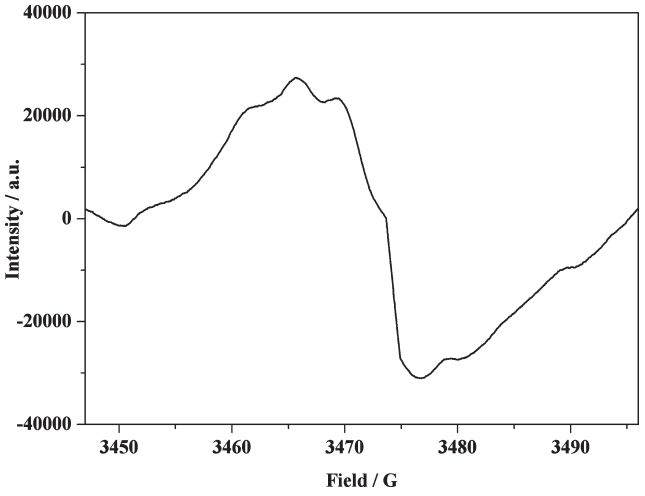

Figure 6. EPR spectrum of powdered MNA with Lande splitting factor g = 2.006.

3.2. EPR Spectra. The exemplary MNA EPR spectrum at RT is shown in Figure 6. The EPR signal intensity in the freshly ground MNA spectrum revealed the concentration 2.52 × 10^{17} spins per gram, one order of magnitude higher than that in the long stored material (6 × 10^{15}).[24] For both nonirradiated and irradiated by NIR samples, the signals lie at g factor 2.006. It may be compared with 2.005, the value considered as unusually high and typical for the charged polarons in n-doped poly-(dithieno[3,4-b:3′,2′-d]thiophene) (PDTT3)[55] and for the nitro radical anions.[56] The effects of NIR irradiation on the MNA powder EPR spectra were examined using two diode lasers: 1550 and 980 nm. The 1550 nm (~6450 cm^{-1}, 0.8 eV) wavelength corresponds to the broad massif at 6600 cm^{-1}(0.82 eV)[24a] and to the combination ν^s_{NH}+ 2 δ^s_{NH} band at 6555 cm^{-1} (0.81 eV),[24b] whereas the 980 nm (~10 200 cm^{-1}, 1.26 eV) beam is not far from the Nd/YAG laser line (1064 nm) exploiting in the SHG measurements, and it corresponds to the second overtone of symmetric stretching $-NH_2$ vibration.[24b] After 0.5 and 3 min of exposure to 980 nm (1 W) laser diode beam, the concentrations were equal to (2.44 and 3.35) × 10^{17} spins/g, respectively. The concentration of spins after 1 and 3 min of exposure to the second diode beam (1550 nm, 50 mW) amounted to (3.20 and 3.40) × 10^{17} spins/g, respectively. Because the negatively charged polarons (radical anions) absorb much lower energy (NIR) than the cations[38] they may couple to overtones or combinational tones. Therefore, the dissociation by direct overtone and combination vibrations excitation is possible and constitutes the autocatalytic process. The decrease in spin concentration after 0.5 min of illumination by the powerful laser diode beam; then, its increase may indicate the initial recombination and further releasing of the charges from traps,[57] their subsequent generation, or both. Because the increase is slightly larger after the weaker beam exposure and our examinations are only qualitative ones the 1550 nm diode was chosen to study the NIR illumination effect on the MNA CD spectra.

3.3. CD Spectra. The CD spectra of MNA solution, of KBr pellet, of MNA single crystal, and of the pellet in chosen orientation before and after 3 min exposure by 1550 nm diode beam were registered in the 340−800 nm region and are shown in Figure 7. The larger spectral range is presented to better

compare them with the theoretical CD spectra depicted in Figure 8. The energy maxima and minima in the calculated spectra of charged clusters (Figure 8d−f) are red-shifted and nearer to the experimental ones (Figure 7) as compared with those of neutral molecule (Figure 8a−c), but their intensities are slightly smaller.

The calculated absorption spectrum for radical anion in crystal (along [102] axis) also reveals very strong shifts toward NIR of all bands in comparison with the MNA neutral molecule; for example, the first transition lies at 3.63 eV (341 nm) in the molecule and at 1.55 eV (797 nm) in the radical anion. The 35% increase in paramagnetic species concentration after 3 min of exposure to 1550 nm beam (previous section) evidences the influence of irradiation. It is especially seen in the CD band at 2.72 eV (457 nm, 21 910 cm^{-1}) corresponding to the low-energy band (presumably of ICT) in Figure 7c for single crystal. It seems that this chirality is induced by motions (conformational chirality) like in the benzophenone crystal.[40] The chirality is also induced by polarons presence due to the spintronic mechanism.[23] The CD induced by spin presence and the magnetic dipole moments connected to rotational strength contributes to the MNA optical nonlinearity. With the large hyperpolarizability of polarons (next subsection), it can elucidate the underestimation of MNA linear susceptibilities by the electrostatic modeling[37] and the discrepancies between calculated and experimental second-order susceptibilities.[58]

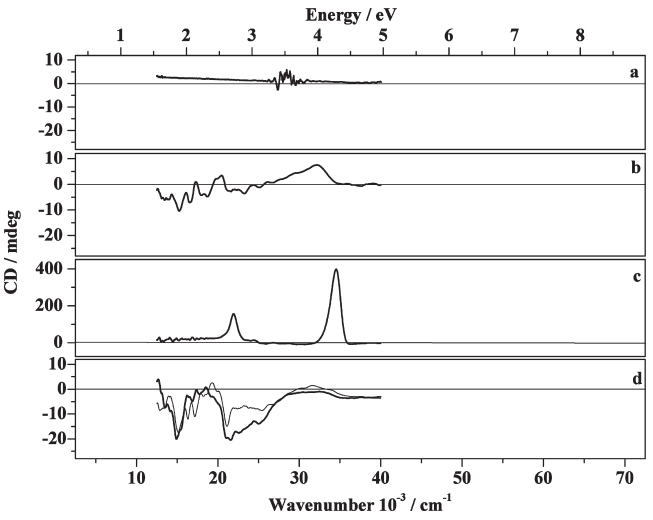

Figure 7. Experimental CD spectra of: (a) MNA solution in spectral grade chloroform (0.026 M), (b) average spectrum from eight different orientations of MNA powder in KBr pellet, (c) average spectrum from five orientations of MNA single crystal, and (d) the pellet in chosen orientation before and after 3 min of exposure to 1550 nm diode beam. Please note the different ordinate scale in part c.

3.4. Hyperpolarizability and Other Properties. The calculated (with optimized geometry) static vectorial hyperpolarizabilities of MNA neutral molecule and radical anion amount to $(1.12 \text{ and } 9.34) \times 10^{-30}$ esu, respectively. The molecular β value is smaller than the experimental one in the 1,4-dioxane solution $(16.7 \pm 0.5) \times 10^{-30}$ esu at 1.060 μm (ref 29); nevertheless, the polaronic β is almost one order of magnitude larger than that of the neutral molecule. The presence of polarons with hyperpolarizability larger than that of neutral molecule in the MNA stable sample and the increase in their number during NIR (e.g., Nd/YAG) irradiation seems to be one of the reasons for large MNA SHG efficiency. It enables us to explain the difference between relative SHG efficiencies of the MNA crystal (1.61) and fine powder (4.35)[59] because the mechanical grinding is also known to generate radical ions.[22] The electric dipole moment (μ) of molecule is equal to 7.01 D (exp. 7.4 ± 0.15 D),[29] and its analog,"μ", in the radical anion is 10.49 D. The last value is similar to 10.69 and 10.86 D found in ref 38 for the first two excited

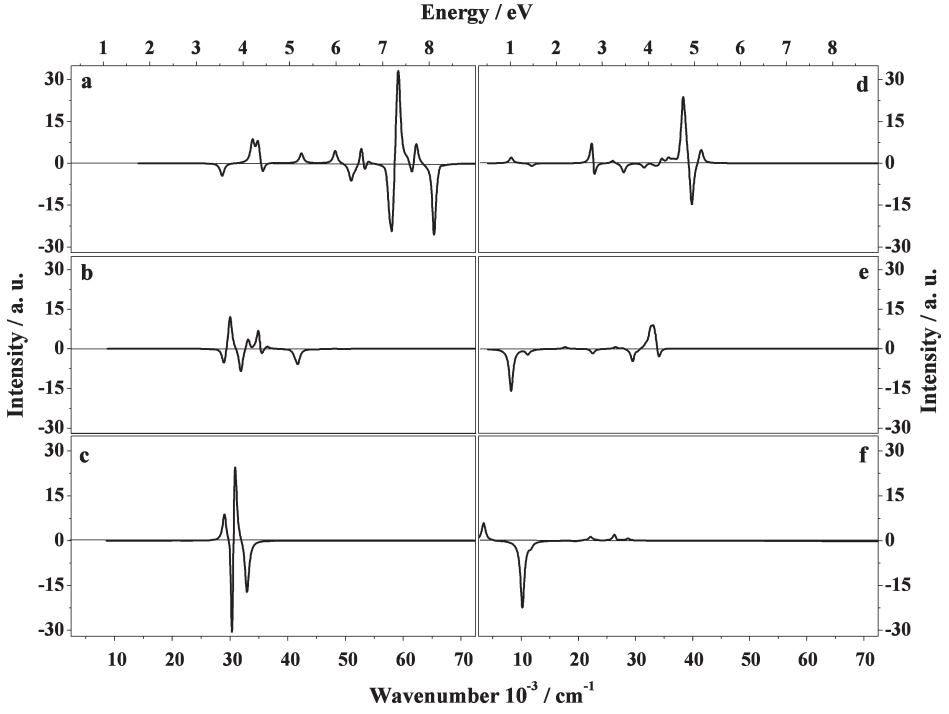

Figure 8. Theoretical CD spectra of: (a) MNA neutral monomer, (b) dimer, and (c) trimer and of: (d) MNA charged monomer, (e) dimer, and (f) trimer, all lying along the [102] helical axis.

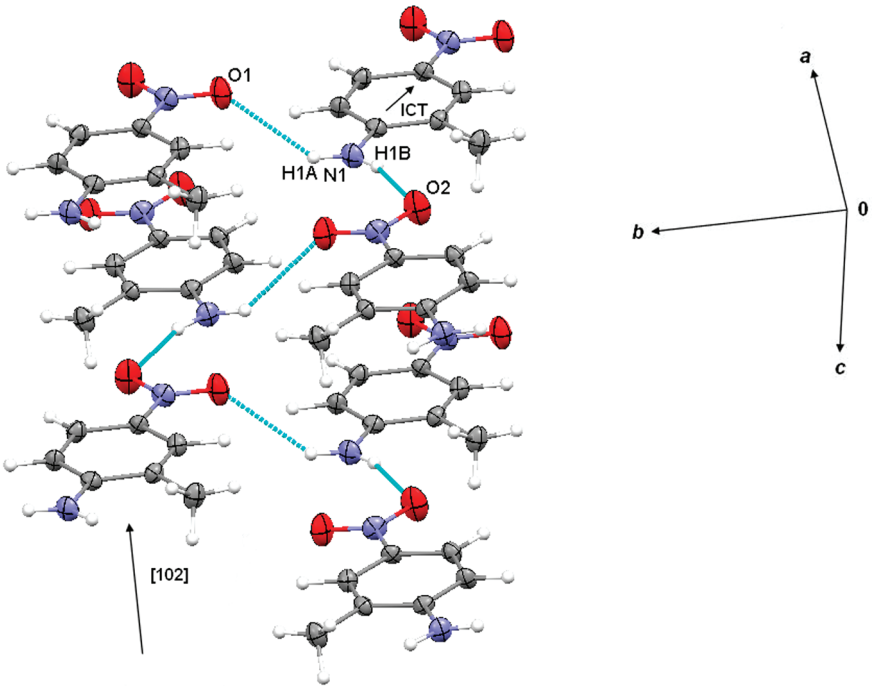

Figure 9. Directions of two N − H···O hydrogen bonds of intramolecular charge transfer (ICT), of crystallographic axes, and of polar [102] axis in MNA crystal.

$\pi-\pi^*$ singlet states, suggesting that the formal charge separations in polarons and these states are also similar.

The IEs and EAs amount to 6.83 and 2.32 eV, respectively, for the molecule and (−0.54 eV(α), +2.09 eV(β)) and (−1.84 eV(α), −1.92 eV(β)) for the radical anion. α and β denote electron spin up (↑) and down (↓), respectively. For the m-NA molecule, IE and EA were equal to 5.39 and 3.14 eV,[21] respectively. Dipole moments, IEs, and EAs for one, two, and three molecule clusters along the polar [102] direction are equal to: (μ): 8.05/18.65/30.08 D; IE: 6.42/5.72/5.53 eV; EA: 1.79/2.62/7.15 eV. The changes of μ with growing size are in accordance with expectation, whereas the trimer's values of IE and EA indicate its easy dissociation. The IE value for helical polythiophene equals 4.68 eV[2] and is comparable to the value for three molecule helical MNA cluster. Corresponding values for negatively charged monomer, dimer, and trimer lying along the polar [102] direction are equal "μ": 10.68/9.58/10.02 D; IE(α,β): (−1.96, +1.28 eV)/(−0.54, +2.69 eV)/(+0.09, +3.32 eV); EA-(α,β): (−4.49, −4.41 eV)/(−1.043, −1.42 eV)/(−0.25, −0.34 eV); and D_0-D_1: 1.17/0.24/0.13 eV, respectively.

3.5. Calculated Band Structure Contradictory with Unmeasurable Electric Conductivity. The valence and conduction bandwidths in the *a*, *b*, and *c* axes directions at $\mathbf{k}\cdot a(b,c) = 0$ (**k**-wave vector) amount to 25.9 and 50.3 meV; 0.3 and 0 meV; and 24.1 and 16.1 meV, respectively. These results reveal the anisotropy of the MNA band structure and the quasi 2D character of its expected conductivity. Along the polar axis [102] direction, for the trimer, the valence and conduction bandwidths are equal to 15 and 29 meV. The calculated energy gaps between the conduction and valence band in the *a*, *b*, and *c* directions are equal to 2.18, 2.23, and 2.21 eV, respectively, and 1.59 eV along the polar axis. Previously computed m-NA crystal band structure with 1.77 eV band gap revealed its 1D conductivity character; the values of bandwidths were similar to those of MNA.[21] In contrast with the m-NA crystal, the MNA one does not reveal electric conductivity.[60] The negative result of MNA-pressed pellet conductivity measurements may be understood by considering the mutual directions of ICT and two distinct N−H···O HBs presented in Figure 9. As can be seen, the two hydrogen atoms of $-NH_2$ group participate in two oppositely directed HBs. The shorter ones form presumable helix (cf. Figure 1), whereas the longest HBs (at the angle ∼140°) connect the two helices in two different layers, forming the extended 3D helix still along [102] axis. The CTs connected to HBs seem to cancel each other to a large extent. Also, ICT from the $-NH_2$ through the phenyl ring to the $-NO_2$ group, creating polar axis [102], does not cooperate with HBs. It seems that the competing interactions prevent the polaron transport and electric conductivity. The efficient nonlinearity of the disordered MNA (at RT) crystal and the negative result of its electric conductivity agree with the finding that the disorder plays a positive role toward NLO properties and a negative role with respect to electrical conductivity.[61,62]

4. CONCLUSIONS

Charged polarons in the MNA crystal may be generated because of the charge separation in the ICT excitons distorted by the multiple phonons (stretching vibrations of the $-NO_2$ and $-NH_2$ groups, some phenyl ring vibrations) and by the NIR irradiation exciting overtones and combination vibrations coupled to intermolecular CTs. The unpaired spins induce CD and enhance NLO properties. Additionally, the atomic motions at RT create conformational helical superstructure, most probably along the polar [102] axis. The oppositely directed two different N − H···O HBs and the dynamic disorder exclude the circulation of charge carriers along the extended helix and thus the electric conductivity of MNA solids.

■ ASSOCIATED CONTENT

Ⓢ Supporting Information. Positions and relative intensities of MNA low frequency and normal vibration bands observed

dx.doi.org/10.1021/jp204168s |*J. Phys. Chem. A* 2011, 115, 7448–7455

in RR spectra. This material is available free of charge via the Internet at http://pubs.acs.org

AUTHOR INFORMATION

Corresponding Author

*Tel: +48 71 3202436. Fax: +48 71 3203364. E-mail: magdalena.m.szostak@pwr.wroc.pl.

ACKNOWLEDGMENT

The numerical calculations have been performed in part at Wrocław Centre for Networking and Supercomputing. We thank MSc. Wojciech Nowak (Faculty of Chemistry, University of Wrocław) for the CD spectra records. This work was sponsored by Wrocław University of Technology under statutory funds no. 343 998.

REFERENCES

(1) Hamada, N.; Sawada, S.; Oshiyama, A. *Phys. Rev. Lett.* **1992**, *68*, 1579.
(2) Ripoll, J. D.; Serna, A.; Guerra, D.; Restrepo, A. *J. Phys. Chem. A* **2010**, *114*, 10917.
(3) Friesen, B. A.; Rich, C. C.; Mazur, U.; McHale, J. L. *J. Phys. Chem. C* **2010**, *114*, 16357.
(4) Zheng, J.; Qiao, W.; Wan, X.; Gao, J. P.; Wang, Z. Y. *Chem. Mater.* **2008**, *20*, 6163.
(5) Heller, E. J. *Acc. Chem. Res.* **1981**, *14*, 368.
(6) Hung, S. T.; Wang, C. H.; Myers Kelley, A. *J. Chem. Phys.* **2005**, *123*, 144503.
(7) Eisfeld, A.; Kniprath, R.; Briggs, J. S. *J. Chem. Phys.* **2007**, *126*, 104904.
(8) Jeanmaire, D. L.; Van Duyne, R. P. *J. Am. Chem. Soc.* **1976**, *98*, 4029.
(9) Hoekstra, R. M.; Zink, J. I.; Telo, J. P.; Nelsen, S. F. *J. Phys. Org. Chem.* **2009**, *22*, 522.
(10) Nelsen, S. F.; Konradsson, A. E.; Weaver, M. N.; Telo, J.P. J. *Am. Chem. Soc.* **2003**, *125*, 12493.
(11) Bailey, S. E.; Zink, J. I.; Nelsen, S. F. *J. Am. Chem. Soc.* **2003**, *125*, 5939.
(12) Albrecht, A. C. *J. Chem. Phys.* **1961**, *34*, 1476.
(13) Carlone, C.; Cyr, C.; Jandl, S.; Truong, K. D.; Hota, N. K.; Zauhar *J. Can. J. Phys.* **1983**, *61*, 1510.
(14) Ando, R. A.; Rodriguez-Redondo, J. L.; Sastre-Santos, A.; Fernandez-Lazaro, F.; Azzellini, G. C.; Borin., A. C.; Santos, P. S. *J. Phys. Chem. A* **2007**, *111*, 13452.
(15) Laska, J. *Mater. Sci. Eng., B* **1999**, *68*, 76.
(16) Kulshreshtha, A. P.; Mookherji, T. *Mol. Cryst. Liq. Cryst.* **1970**, *10*, 75.
(17) Szostak, M. M.; Jakubowski, B.; Komorowska, M. *Mol. Cryst. Liq. Cryst.* **1993**, *229*, 7.
(18) Wang, Z. J.; Zhang, J.; Wu, X.; Birau, M.; Yu, G.; Yu, H.; Qi, Y.; Desjardins, P.; Meng, X.; Gao, J. P.; Todd, E.; Song, N.; Bai, Y.; Beaudin, A. M. R.; LeClair, G. *Pure Appl. Chem* . **2004**, *76*, 1435.
(19) Szostak, M. M.; Wójcik, G.; Gallier, J.; Bertault, M.; Freundlich, P.; Kołodziej, H. A. *Chem. Phys.* **1998**, *229*, 275.
(20) Szostak, M. M.; Czarnecki, M. A. *Pol. J. Chem.* **2002**, *76*, 419.
(21) Szostak, M. M.; Chojnacki, H.; Staryga, E.; Dłużniewski, M.; Bąk, G. *Chem. Phys.* **2009**, *365*, 44.
(22) Szostak, M. M.; Chojnacki, H. *Opt. Mater.* **2011**, *33*, 1395.
(23) Joshua, A.; Venkataraman, V. *J. Phys.:Condens. Matter* **2009**, *21*, 445804.
(24) (a) Okwieka, U.; Szostak, M. M.; Misiaszek, T; Turowska-Tyrk, I.; Natkaniec, I.; Pavlukojć, A. *J. Raman Spectrosc.* **2008**, *39*, 849. (b) Okwieka, U. Ph.D. Thesis, Wroclaw University of Technology, Wrocław, Poland, 2008.
(25) Levine, B. F.; Bethea, C. G.; Thurmond, C. D.; Lynch, R. T.; Bernstein, J. L. *J. Appl. Phys.* **1979**, *50*, 2523.
(26) Lipscomb, G. F.; Garito, A. F.; Narang, R. S. *J. Chem. Phys.* **1981**, *75*, 1509.
(27) Ho, E. S. S.; Iizuka, K.; Freundorfer, A. P.; Wah, C. K. L. *J. Appl. Phys.* **1991**, *69*, 1173.
(28) Zyss, J.; Oudar, J. L. *Phys. Rev. A* **1982**, *26*, 2028.
(29) Bosshard, Ch.; Knöpfle, G.; Prdtre, P.; Günter, P. *J. Appl. Phys.* **1992**, *71*, 1594.
(30) Ferguson, G.; Glidewell, C.; Low, J. N.; Skakle, J. M. S.; Wardell, J. L. *Acta Crystallogr., Sect. C* **2001**, *57*, 315.
(31) Howard, S. T.; Hursthouse, M. B.; Lehmann, C. W.; Mallinson, P. R.; Frampton, C. S. *J. Chem. Phys.* **1992**, *97*, 5616.
(32) Whitten, A. E.; Turner, P.; Klooster, W. T.; Piltz, R. O.; Spackman, M. A. *J. Phys. Chem. A* **2006**, *110*, 8763.
(33) Hamada, T. *Chem. Phys.* **1986**, *100*, 8777.
(34) Castet, F.; Champagne, B. *J. Phys. Chem. A* **2001**, *105*, 1366.
(35) Guillaume, M.; Botek, E.; Champagne, B.; Castet, F.; Ducasse., L. *Int. J. Quantum Chem.* **2002**, *90*, 1378.
(36) Cheng, W.-D.; Wu, D.-S.; Zhang, H.; Li, X.-D.; Chen, D.-G.; Lang, Y.-Z.; Gong, Y.-J. *J. Phys. Chem. B* **2004**, *108*, 12658.
(37) Kanoun, M. B.; Botek, E.; Champagne, B. *Chem. Phys. Lett.* **2010**, *487*, 256.
(38) Szostak, M. M.; Kozankiewicz, B.; Lipiński, J. *Spectrochim. Acta A* **2007**, *6*, 1412.
(39) Okwieka, U.; Hołderna-Natkaniec, K.; Misiaszek, T.; Medycki, W.; Baran, J.; Szostak, M. M. *J. Chem. Phys.* **2009**, *131*, 144505.
(40) Matsuura, T.; Koshima, H. *J. Photochem. Photobiol., C* **2005**, *6*, 7.
(41) Sakamoto, M. *J. Photochem. Photobiol., C* **2006**, *7*, 183.
(42) Jerphagnon, J.; Chemla, D. S. *J. Chem. Phys.* **1976**, *65*, 1522.
(43) Szostak, M. M.; Kozankiewicz, B.; Wojcik, G.; Lipiński, J. *J. Chem. Soc., Faraday Trans.* **1998**, *94*, 3241.
(44) Di Bella, S.; Fragala, I.; Marks, T. J.; Ratner, M. A. *J. Am. Chem. Soc.* **1996**, *118*, 12747.
(45) Shimizu, A.; Mori, T.; Inoue, Y.; Yamada, S. *J. Phys. Chem. A* **2009**, *113*, 8754.
(46) Frisch, M. J.; Trucks, G. W.; Schlegel, H. B.; Scuseria, G. E.; Robb, M. A.; Cheeseman, J. R.; Scalmani, G.; Barone, V.; Mennucci, B.; ,Petersson, G. A.; Nakatsuji, H.; Caricato, M.; Li, X.; Hratchian, H. P.; ,Izmaylov, A. F.; Bloino, J.; Zheng, G.; Sonnenberg, J. L.; Hada, M.; ,Ehara, M.; Toyota, K.; Fukuda, R.; Hasegawa, J.; Ishida, M.; Nakajima, T.; Honda, Y.; Kitao, O.; Nakai, H.; Vreven, T.; Montgomery, J. A., Jr.; Ogliaro, F.; Bearpark, M.; Heyd, J. J.; Brothers, E.; ,Kudin, K. N.; Staroverov, V. N.; Kobayashi, R.; Normand, J.; Raghavachari, K.; Rendell, A.; Burant, J. C.; Iyengar, S. S.; Tomasi, J.; ,Cossi, M.; Rega, N.; Millam, J. M.; Klene, M.; Knox, J. E.; Cross, J. B.; ,Bakken, V.; Adamo, C.; Jaramillo, J.; Gomperts, R.; Stratmann, R. E.; ,Yazyev, O.; Austin, A. J.; Cammi, R.; Pomelli, C.; Ochterski, J. W.; Martin, R. L.; Morokuma, K.; Zakrzewski, V. G.; Voth, G. A.; ,Salvador, P.; Dannenberg, J. J.; Dapprich, S.; Daniels, A. D.; ,Farkas, O.; Foresman, J. B.; Ortiz, J. V.; Cioslowski, J.; Fox, D. J. *Gaussian 09*, revision A.02; Gaussian, Inc.: Wallingford, CT, 2009.
(47) Neese, F. *Lehrstuhl fuer Theoretische Chemie*; Institut fuer Physikalische und Theoretische Chemie, Universitaet Bonn: Bonn, Germany 2010.
(48) Nakajima, T.; Nakatsuji, H. *Chem. Phys. Lett.* **1997**, *280*, 79.
(49) (a) Manne, R. *Chem. Phys. Lett.* **1968**, *8*, 230.(b) Manne, R.; Chojnacki, H. *JACOMP Package*; Uppsala University: Uppsala, Sweden, 1974.
(50) Varsányi, G. *Vibrational Spectra of Benzene Derivatives*; Akadémiai Kiadó: Budapest, Hungary, 1969.
(51) Heimel, G.; Somitsch, D.; Knoll, P.; Brédas, J.-L.; Zajer, E. *J. Chem. Phys.* **2005**, *122*, 114511.
(52) Tokura, Y.; Kurita, A.; Koda, T. *Phys. Rev. B* **1985**, *31*, 2588.
(53) Teng, C. C.; Garito, A. F. *Phys. Rev. B* **1983**, *28*, 6766.
(54) Zink, J. I.; Shin, S. K. In *Advances in Photochemistry*; Volman, D. H., Hammond, G. S., Neckers, D. C., Eds.; John Wiley & Sons: Hoboken, NJ, 1991, Vol. 16.

(55) Cravino, A.; Neugebauer, H.; Luzzati, S.; Catellani, M.; Petr, A.; Dunsch, L.; Sariciftci, N. S. *J. Phys. Chem. B* **2002**, *106*, 3583.
(56) Filipiak, P.; Camaioni, D. M.; Fessenden, R. W.; Hug, G. L. *J. Phys. Chem. B* **2006**, *110*, 11046.
(57) Rohrbacher, H.; Karl, N. *Phys. Status Solidi A* **1975**, *29*, 517.
(58) Kanoun, M. B.; Champagne, B. *Int. J. Quantum Chem.* **2011**, *111*, 880.
(59) Yang, G.; Li, Y.; Dreger, Z. A.; White, J. O.; Drickamer, H. G. *Chem. Phys. Lett.* **1997**, *280*, 375.
(60) Dłużniewski, M.; Bąk, G. W. Unpublished negative results of the conductivity measurements on MNA 3 mm thick pellet pressed under 8 ton·cm^{-2} (8 kbar) pressure.
(61) Makowska-Janusik, M.; Tkaczyk, S.; Kityk, I. V. *J. Phys. Chem. B* **2006**, *110*, 6492.
(62) Mereau, R.; Castet, F.; Botek, E.; Champagne, B. *J. Phys. Chem. A* **2009**, *111*, 6552.